Multimodal Image Fusion Method Based on Multiscale Image Matting

Sarmad Maqsood[1], Robertas Damasevicius[1(✉)], Jakub Siłka[2], and Marcin Woźniak[2]

[1] Department of Software Engineering, Kaunas University of Technology, Kaunas, Lithuania
{sarmad.maqsood,robertas.damasevicius}@ktu.lt
[2] Faculty of Applied Mathematics, Silesian University of Technology, Gliwice, Poland
marcin.wozniak@polsl.pl

Abstract. Multimodal image fusion combines the complementary information of multimodality images into a single image that preserves the information of all the source images. This paper proposes a multimodal image fusion method situated on image enhancement, edge detection, multiscale sliding window, and image matting to obtain the detailed region information of the input images. In the proposed system, firstly the multimodality input images are rectified via a contrast enhancement method through which the intensity distribution is refined for clear vision. The spatial gradient edge detection method is utilized for separating the edge information from the contrast-enhanced images. These edges are then used by a multiscale sliding window method to provide global and local activity level maps. These activity maps further generate trimap and decision maps. Finally, by employing the improved decision maps and fusion rule the fused image is acquired.

Keywords: Multimodal medical image · Image fusion · Multiscaling · Image matting

1 Introduction

Multimodality image fusion combines important information from various imaging modalities to provide an improved fused image. The obtained fused image is highly informative and is very dedicated to further processing for disease diagnosis and remedy [1,2]. Multimodal image fusion techniques have an extensive variety of applications for their improved and precise illustration of informative outcomes [3,5,6]. Diversified medical modalities i.e., CT and MRI that have allowed radiologists to analyze the important body patterns and parts positioned in the internal human body for reports generating and clinical analysis [7–9]. Therefore, multimodal images of various modalities are needed to be merged to produce a single image that can allow functional information. To obtain the fused image with significant details has drawn researchers attention to multimodal fusion of medical images [4,10].

L. Rutkowski et al. (Eds.): ICAISC 2021, LNAI 12855, pp. 57–68, 2021.
https://doi.org/10.1007/978-3-030-87897-9_6

Image fusion normally has two core divisions, one is the spatial domain the other is the transform domain [11]. The spatial domain technique produces the fused image by taking pixels/sections/blocks of images deprived of alteration [12]. Transform domain techniques merge the complementary transform coefficients and apply an inverse transformation to form the image fusion. Many research present also machine learning models [13].

The multiscale transformation fusion method has great attention in medical image fusion. In transform domain-based technique, variational adaptive PDE [14], contourlet transform [15], discrete wavelet transform [16], non-subsampled contourlet transform [17], curvelet transform [18] and sparse representation [11] methods have been employed in multimodal image fusion. In the current intervals, numerous image fusion approaches have been presented i.e., multiscale and optimization-based image fusion. Multiscale approaches give detailed images representation, these techniques well preserve the details of the edge [2]. Multiscale transformation and sparse representation methods have obtained a significant interest in the transform domain and work positively in the analysis of medical images [19]. However, these methods exhibit several limitations, i.e., undesirable side effects such as reduced contrast and high spatial distortion, the appearance of artifacts in the fused images.

This paper proposes a multimodal image fusion approach using contrast enhancement and edge detection method to extract the edges from the input images. A multiscale sliding window technique is employed for identifying the global and local intensity alterations to produce the initial activity level maps. These various activity level maps then create a trimap. An improved image matting method is employed for creating the final decision maps. Finally, by using the enrich decision maps and fusion rule the fused image is formed.

The remaining paper is structured as follows. Section 2 explains the detailed method of the proposed framework. Section 3 presents the fusion metrics. The experiment results and discussion are presented in Sect. 4 and finally conclusion is given in Sect. 5.

2 The Proposed Multiscaling Image Matting (MSIM) Technique

Let, I_i is the source image with dimensions of $R \times S$, where $r = 1, 2, 3, \ldots, R$, $s = 1, 2, 3, \ldots, S$ and $i \in [1, 2]$ shows the CT and MR images, respectively. The proposed MSIM fusion method is detailed in Algorithm 1.

Algorithm 1. Proposed multimodal image fusion framework

Input Image: $I_i, i \in [1, 2]$.
Output Image: Fused Image I_F.
begin
Improve contrast, $I_i \xrightarrow{\text{contrast enhancement}} \acute{I}_i$.
Compute edges, B_p and $B_q \xrightarrow{\text{edge maps}} B_i$.
for k = 9, l = 9 **do**
  Compute activity maps, w, $B_i \xrightarrow{9 \times 9} \acute{G}_i$.
  Compute smooth activity maps, $\acute{G}_i \xrightarrow{\text{sum filter}} G_i$.
  Compute score maps, $G_i \rightarrow \xi_1$.
end for
for k = 27, l = 27 **do**
  Compute activity maps, w, $B_i \xrightarrow{27 \times 27} \acute{H}_i$.
  Compute smooth activity maps, $\acute{H}_i \xrightarrow{\text{sum filter}} H_i$.
  Compute score maps, $H_i \rightarrow \xi_2$.
end for
Compute focus maps, $\xi_{1,2} \xrightarrow{\text{AND}} D_1$ and D_2.
Generate trimap, $D_{1,2} \xrightarrow{\text{trimap}} T$.
Create alpha matte, T, $I_i \xrightarrow{\text{matting}} \alpha$.
Obtain fused image, $I_F = \alpha \times I_i$.
end

2.1 Preprocessing

Contrast enhancement is the most extensive method to improve the images having low contrast. No-reference image quality assessment (NR-IQA) [20], is employed to refine the contrast and conserve the mean brightness of the input images I_i.

$$\acute{I}_i \xleftarrow{\text{NR-IQA [20]}} I_i. \tag{1}$$

I_i is employed to the input images to get the contrast enhanced images $\acute{I}_i$. Image enhancement improved the edges of both source images. Figure 1 illustrates the improvement in edge information. Figure 1 (a, b) shows the source images of CT and MR images, respectively, and their map edges are displayed in Fig. 1 (c, d). Contrast enhancements of CT and MR images are illustrated in (Fig. 1 (e, f)) and their corresponding gradient maps are displayed in Fig. 1 (g, h). It is worth mentioning that after the contrast enhancement approach, there is a prominent improvement in the edges of the source images.

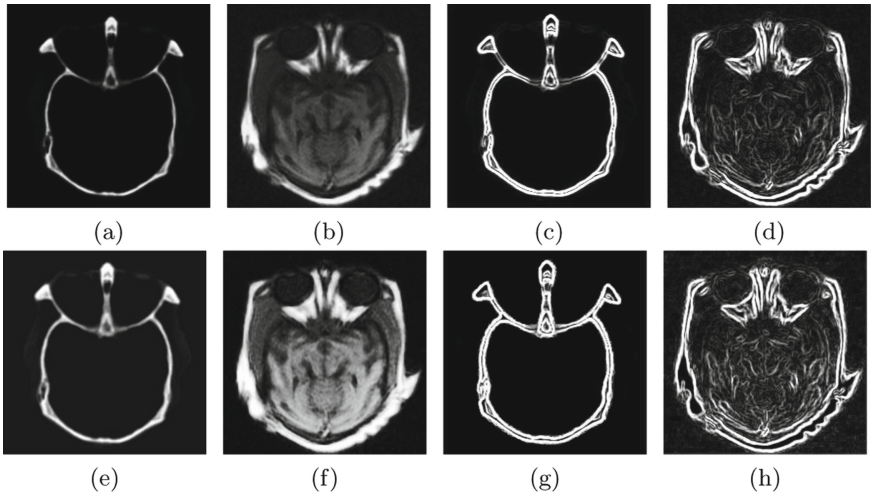

Fig. 1. The "CT and MRI" input images for edge detection after image enhancement. (a, b) Input images, (c, d) edges of (a, b) achieved by sobel operator [21], (e, f) contrast enhancement using No-reference image quality assessment (NR-IQA) [20], (g, h) edges of (e, f) attained by sobel operator.

2.2 Feature Extraction

The Sobel Operator [21] is used to achieve the edges of an image by calculating an approximation of an image gradient. At each location the result is either the norm of this vector or corresponding gradient vector.

Firstly, the gradient is obtained in X direction by convolving the image with the first kernel from left to right given in Eq. (2) as,

$$B_p = \begin{bmatrix} 1 & 0 & -1 \\ 2 & 0 & -2 \\ 1 & 0 & -1 \end{bmatrix}. \tag{2}$$

Similarly, the image is convoluted with the first kernel from top to bottom and the gradient is obtained in Y direction given in Eq. (3) as,

$$B_q = \begin{bmatrix} 1 & 2 & 1 \\ 0 & 0 & 0 \\ -1 & -2 & -1 \end{bmatrix}. \tag{3}$$

At this point the vectors of the gradient of image are obtained. The magnitude of each vector B_i is calculated by using Eq. (4) to obtain the edges.

$$B_i = \sqrt{(B_p)^2 + (B_q)^2}. \tag{4}$$

2.3 Multiscaling

A multiscale sliding window method is employed to obtain various salient features from activity maps B_i. The windows which are created for this experiment are 9×9 and 27×27. Firstly, by applying the spatial domain filters the activity maps are classified into a set of 9×9 components, as given Eq. (5) and Eq. (6):

$$\acute{G}_i(r,s) = \sum_{a=-k}^{k} \sum_{b=-l}^{l} w(a,b) B_i(x+a, y+b). \tag{5}$$

$$G_i(u,v) = \sum_{(r,s)\epsilon\Omega} \acute{G}_i(r,s). \tag{6}$$

Each set activity is preserved in the map scores form. Moreover, the intensity values calculated in each block ($G_1(u,v)$ and $G_2(u,v)$) is deliberated to improve the score maps ξ_a^1 and ξ_b^1 by compared with one another as in Eq. (7) and Eq. (8).

$$\xi_a^1(r,s) = \begin{cases} 1, & \text{if } G_1(u,v) > G_2(u,v) \\ 0, & \text{Otherwise} \end{cases} \tag{7}$$

$$\xi_b^1(r,s) = 1 - \xi_a^1(r,s). \tag{8}$$

Similarly, the activity map for 27×27 block of pixels is given as in Eq. (9) and Eq. (10).

$$\acute{H}_i(r,s) = \sum_{a=-(k\times 3)}^{k\times 3} \sum_{b=-(l\times 3)}^{l\times 3} w(a,b) B_i(x+a, y+b). \tag{9}$$

$$H_i(u,v) = \sum_{(r,s)\ \epsilon\ \Omega} \acute{H}_i(r,s). \tag{10}$$

Each block size activity is also preserved in the map scores form. The intensity levels calculated in each 27×27 block ($H_1(u,v)$ and $H_2(u,v)$) is deliberated to improve the score maps ξ_a^2 and ξ_b^2 by compared with one another as in Eq. (11) and Eq. (12).

$$\xi_a^2(r,s) = \begin{cases} 1, & \text{if } H_1(u,v) > H_2(u,v) \\ 0, & \text{Otherwise} \end{cases} \tag{11}$$

$$\xi_b^2(r,s) = 1 - \xi_a^2(r,s). \tag{12}$$

The different sliding windows maps provide different features information which refine the maps quality. The information from the input images at various scales are selected by multiscale sliding windows technique and provide disparate information for image fusion i.e., small window size extracts local characteristics and large window size focuses on global intensity variations of an image. The multiscale information of all maps (ξ_a^1 and ξ_a^2) and (ξ_b^1 and ξ_b^2) are fused together to form a single focus map, conveying the features of both scales as given in Eq. (13).

$$D_i(r,s) \xleftarrow{\text{AND}} \xi_b^i(r,s), \xi_b^i(r,s). \tag{13}$$

After that the trimap is generated. It roughly divides the input images into following regions i.e., definite focused, definite defocused and the unknown regions. The trimap T is processed by using D_1, D_2 as in Eq. (14).

$$T \xleftarrow{\text{Trimap}} D_i. \tag{14}$$

The trimap (T), source images (I_1, I_2) are combined to construct an alpha matte (α) by using the closed-form matting technique [22], as in Eq. (15).

$$\alpha \xleftarrow{\text{Alpha Matte}} T, I_i. \tag{15}$$

where α is a value between [0, 1], which means that these pixels are mixed by the focused and defocused pixels. $\alpha(r,s) = 1$ or 0 means that the point (r,s) of the source image A_i is in the focus or defocus, respectively. Finally, the fused image is formed by calculating the weighted sum of the source image with alpha matte performed as a weight map as in Eq. (16).

$$I_F(r,s) = \sum_{n=1:i} \alpha(r,s) \times I_i(r,s). \tag{16}$$

3 Objective Evaluation Metrics

To assess the superiority and the effectiveness of the proposed MSIM system with others image fusion algorithms, five most commonly metrics are used for quantitative analysis, i.e., Mutual Information (MI) [23], Entropy (EN) [24], Feature Mutual Information (FMI) [25], Spatial Structural Similarity (SSS) [26], and Visual Information Fidelity (VIF) [27]. For these metrics, the bold value exhibits the higher result. These metrics are defined as follows.

3.1 Mutual Information (MI)

MI [23] calculates the mutual information between two discrete variables and is defined as,

$$MI = \sum_{x=1}^{n}\sum_{y=1}^{n} H_{ij}(x,y)\log_2 \frac{H_{ij}(x,y)}{H_i(x)H_j(y)}, \tag{17}$$

where H_{ij} (x, y) shows the combined probability density distribution of the grayscale image in i and j. $H_i(x)$ and $H_j(y)$ shows the probability density distribution of the grayscale image in i and j, respectively. It calculates the sum of common information among source images and the fused image. Highest MI value reveals that the fused image has more information than the source images.

3.2 Entropy (EN)

The EN [24] is expressed as,

$$EN(x) = -\sum_{x=0}^{N-1} H_i(x)\log_2 H_i(x), \tag{18}$$

where N is the number of gray level, which is fixed to 256 in this test, and $H_i(x)$ is the normalized histogram of fused image i.

3.3 Feature Mutual Information (FMI)

FMI [25] is determined as,

$$FMI_y^{i,j} = \frac{1}{N}\sum_{x=1}^{N} \frac{I_x(y,i)}{S_x(y)S_x(i)} + \frac{I_x(y,j)}{S_x(y)+S_x(j)}, \tag{19}$$

where N shows sliding windows number, $S_x(y)$ is the entropy of n^{th} window in an image y, $I_x(y, i)$ is the regional common information between n^{th} window of image y and i. Similarly, $I_x(y, j)$ is the regional mutual information between the n^{th} window of image y and j. $FMI_y^{i,j}$ computes the source images edge information. Greater value of $FMI_y^{i,j}$ shows the better fused image quality.

3.4 Spatial Structural Similarity (SSS) $Q^{AB/F}$

$Q^{AB/F}$ SSS [26] is presented by Xydeas and Petrovic. This metric decides the quantity of transmitted information of edges from input images into the fused image. $Q^{AB/F}$ for the two source images can be stated as follow:

$$Q^{AB/F} = \frac{\sum_{l=1}^{m}\sum_{w=1}^{n}(Q^{AB}(p,q)W^A(p,q) + Q^{BF}(p,q)W^B(p,q))}{\sum_{l=1}^{m}\sum_{w=1}^{n}(W^A(p,q) + W^B(p,q))}, \tag{20}$$

where $Q^{AB/F}$ (p, q) denotes the information moves from source image A into the fused image F for the pixel location (p, q) and $W^B(p, q))$ is the weight for a pixel location (p, q). The pixel with higher gradient value influences more to the $Q^{AB/F}$ than the lower gradient value. Thus $W^A(p, q) = [Grad(x, y)]^T$. Where T is a constant.

3.5 Visual Information Fidelity (VIF)

VIF [27] is developed on human visual system. VIF evaluates the performance of fusion between the source image and the fused image by calculating the data common among them. In most possibility, a standard source image is hard to achieve. To estimate the fusion performance in this experiment an adapted model of VIF, is determined between the source images and the fused result by averaging the values of VIF.

4 Results and Discussion

4.1 Experimental Setup

In this section, the proposed image fusion approach is compared both subjectively and objectively with three image fusion methods, i.e., Guided Filtering based fusion (GFF) [28], Laplacian Pyramid (LP) [29] and Convolutional Neural Network (CNN) [30]. All the aforementioned approaches are implemented based upon the codes available by the authors. The medical image fusion datasets are acquired from [31] and the dimensions of the source images standardized as 256 $\times$ 256 pixels. The experiments were performed on a laptop Intel(R) Core i7 2.59 GHz processor with 16 GB RAM using MATLAB R2020b. The proposed MSIM method is analyzed by performing both qualitative and quantitative evaluation processes.

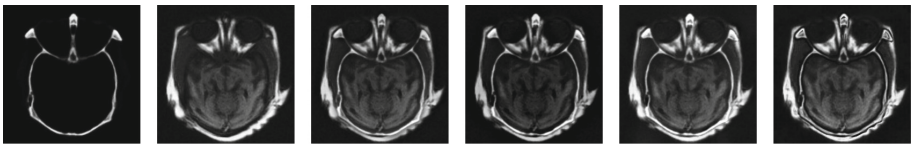

(a) (b) (c) (d) (e) (f)

Fig. 2. Source images "Med-1" and the fused images acquired by different fusion algorithms. (a, b) Source images. (c)–(f) Fused images acquired using GFF [28], LP [29], CNN [30] and proposed method respectively.

4.2 Fusion Results

Three sets of multimodal images are used in this experiment. Figures 2(a, b), 3(a, b), 4(a, b) displayed the source images and the fused results achieved by GFF, LP, CNN, and the proposed method are displayed in Figs. 2(c)–(f), 3(c)–(f), 4(c)–(f) respectively. The source CT image provides the information about bone structures and hard tissues and MRI source image provides soft tissue information. Figures 2(c), 3(c), 4(c) shows the results obtained by GFF, which is unable to fully preserved the information in the fused image because of over enhances the structural features and fail to identify salient brain structures. Figures 2(d), 3(d), 4(d) displayed the results acquired by LP. This approach also

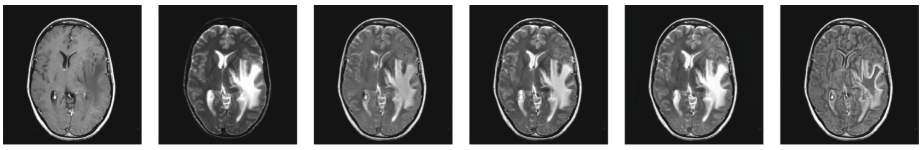

(a) (b) (c) (d) (e) (f)

Fig. 3. Source images "Med-2" and the fused images acquired by different fusion algorithms. (a, b) Source images. (c)–(f) Fused images acquired using GFF [28], LP [29], CNN [30] and proposed method respectively.

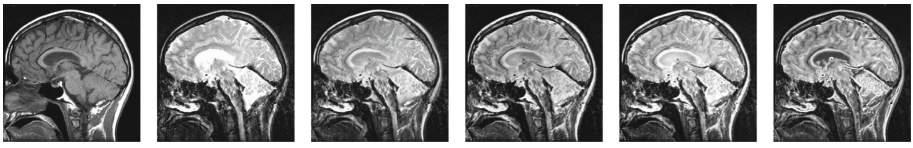

(a) (b) (c) (d) (e) (f)

Fig. 4. Source images "Med-3" and the fused images acquired by different fusion algorithms. (a, b) Source images. (c)–(f) Fused images acquired using GFF [28], LP [29], CNN [30] and proposed method respectively.

Table 1. The quantitative evaluation of different fusion algorithms. Bold values show the highest result.

Images	Fusion methods	MI [23]	EN [24]	FMI [25]	SSS [26]	VIF [27]
Med-1	GFF [28]	3.4313	6.7971	0.9032	0.7849	0.4864
	LP [29]	2.5508	6.2724	0.7412	0.6321	0.4141
	CNN [30]	3.5248	6.7541	0.7712	0.7992	0.8991
	Proposed MSIM	**3.8554**	**6.9324**	**0.9539**	**0.8013**	**0.9342**
Med-2	GFF [28]	3.8595	5.8459	0.8596	0.5919	0.4295
	LP [29]	3.5908	5.6692	0.8568	0.6571	0.4352
	CNN [30]	4.2014	7.8421	0.7458	0.6969	0.8015
	Proposed MSIM	**4.6387**	**8.0138**	**0.8759**	**0.7132**	**0.8583**
Med-3	GFF [28]	3.4514	4.4081	0.9047	0.6470	0.4961
	LP [29]	3.4733	4.6547	0.7690	0.6391	0.9255
	CNN [30]	4.2540	5.1748	0.8421	0.7441	0.9408
	Proposed MSIM	**4.5982**	**5.7483**	**0.9641**	**0.7949**	**0.9822**

failed to detect the structural details information in the fused image and suffers from undesirable artifacts. Figures 2(e), 3(e), 4(e) shows the results obtained by CNN, which provides slightly better results than the remaining methods, but still shows the lack of sharpness and distorted regions. The results of the proposed

method are displayed in Figs. 2(f), 3(f), 4(f) which provides high contrast, clear information and fully preserved the details in the fused image. Table 1 illustrates that the proposed MSIM method also exhibits superior performance quantitatively than the other algorithms. The top value of evaluation metrics shows in the bold highlighted.

5 Conclusions

In this paper, a constructive multimodality image fusion approach is proposed using the Sobel operator and sliding window method to detect the salient pixels of each input image. The input images are firstly pre-processed using the no reference image quality assessment (NR-IQA) contrast enhancement method and their gradients are computed using the Sobel operator. Afterward, the multiscale sliding window method is proposed for the perfect creation of trimap. Then an image matting method is employed to get the accurate region for the decision maps, and the fused images. More importantly, the closed-form matting method is adept to construct full use of the spatial connections between the nearby pixels for weight estimation. The proposed method achieved the highest mutual information, entropy, feature mutual information, spatial structural similarity, and visual information fidelity of 4.638, 8.013, 0.964, 0.801, and 0.982 respectively. Experimental results demonstrate that the proposed image fusion approach well preserves the complementary information of various source images and achieves superior fusion performance both subjectively and objectively when compared with other image fusion algorithms.

References

1. Muzammil, S.R., Maqsood, S., Haider, S., Damaševičius, R.: CSID: a novel multimodal image fusion algorithm for enhanced clinical diagnosis. Diagnostics **10**(11), 904 (2020)
2. Maqsood, S., Javed, U., Riaz, M.M., Muzammil, M., Muhammad, F., Kim, S.: Multiscale image matting based multi-focus image fusion technique. Electronics **9**(2), 472 (2020)
3. Grycuk, R., Wojciechowski, A., Wei, W., Siwocha, A.: Detecting visual objects by edge crawling. J. Artif. Intell. Soft Comput. Res. **10**(3), 223–237 (2020)
4. Grycuk, R., Najgebauer, P., Kordos, M., Scherer, M.M., Marchlewska, A.: Fast image index for database management engines. J. Artif. Intell. Soft Comput. Res. **10**(2), 113–123 (2020)
5. Woźniak, M., Wieczorek, M., Siłka, J., Połap, D.: Body pose prediction based on motion sensor data and recurrent neural network. IEEE Trans. Ind. Inform. **17**(3), 2101–2111 (2020)
6. Juočas, L., Raudonis, V., Maskeliūnas, R., Damaševičius, R., Woźniak, M.: Multifocusing algorithm for microscopy imagery in assembly line using low-cost camera. Int. J. Adv. Manufact. Technol. **102**(9), 3217–3227 (2019). https://doi.org/10.1007/s00170-019-03407-9

7. Guo, Z., Li, X., Huang, H., Guo, N., Li, Q.: Deep learning-based image segmentation on multimodal medical imaging. IEEE Trans. Radiat. Plasma Med. Sci. **3**(2), 162–169 (2019)
8. Ke, Q., Zhang, J., Wei, W., Damaševičius, R., Wozniak, M.: Adaptive Independent Subspace Analysis (AISA) of Brain Magnetic Resonance Imaging (MRI) data. IEEE Access **7**(1), 12252–12261 (2019)
9. Khan, M.A., et al.: Multimodal brain tumor classification using deep learning and robust feature selection: a machine learning application for radiologists. Diagnostics **10**(8), 1–19 (2020)
10. Manchanda, M., Sharma, R.: An improved multimodal medical image fusion algorithm based on fuzzy transform. J. Vis. Commun. Image Represent. **51**(2), 76–94 (2018)
11. Maqsood, S., Javed, U.: Biomedical signal processing and control multi-modal medical image fusion based on two-scale image decomposition and sparse representation. Biomed. Sig. Process. Control **57**, 101810 (2020)
12. Li, H., Qiu, H., Yu, Z., Li, B.: Multifocus image fusion via fixed window technique of multiscale images and non-local means filtering. Sig. Process. **138**, 71–85 (2017)
13. Woźniak, M., Siłka, J., Wieczorek, M.: Deep neural network correlation learning mechanism for CT brain tumor detection. Neural Comput. Appl., 1–16 (2021). https://doi.org/10.1007/s00521-021-05841-x
14. Wei, W., Zhou, B., Połap, D., Woźniak, M.: A regional adaptive variational PDE model for computed tomography image reconstruction. Pattern Recogn. **92**, 64–81 (2019)
15. Yang, S., Wang, M., Jiao, L., Wu, R., Wang, Z.: Image fusion based on a new contourlet packet. Inf. Fusion **11**(2), 78–84 (2010)
16. Yang, Y.: A novel DWT based multi-focus image fusion method. Procedia Eng. **24**(1), 177–181 (2011)
17. Li, H., Qiu, H., Yu, Z., Zhang, Y.: Infrared and visible image fusion scheme based on NSCT and low-level visual features. Infrared Phys. Technol. **76**, 174–184 (2016)
18. Nencini, F., Garzelli, A., Baronti, S., Alparone, L.: Remote sensing image fusion using the curvelet transform. Inf. Fusion **8**(2), 143–156 (2007)
19. Yang, B., Li, S.: Visual attention guided image fusion with sparse representation. Optik (Stuttg) **125**(17), 4881–4888 (2014)
20. Yan, J., Li, J., Fu, X.: No-reference quality assessment of contrast-distorted images using contrast enhancement. arXiv preprint arXiv:1904.08879 (2019)
21. Gao, W., Zhang, X., Yang, L., Liu, H.: An improved Sobel edge detection. In: Proceedings of the 3rd International Conference on Computer Science and Information Technology, vol. 9, no. 11, pp. 67–71 (2010)
22. Levin, A., Lischinski, D., Weiss, Y.: A closed-form solution to natural image matting. IEEE Trans. Pattern Anal. Mach. Intell. **30**(2), 228–242 (2007)
23. Hossny, M., Nahavandi, S., Vreighton, D.: Comments on information measure for performance of image fusion. Electron. Lett. **44**(18), 1066–1067 (2008)
24. Liu, Y., Liu, S., Wang, Z.: A general framework for image fusion based on multiscale transform and sparse representation. Inf. Fusion **24**, 147–164 (2015)
25. Haghighat, M.B.A., Aghagolzadeh, A., Seyedarabi, H.: A non-reference image fusion metric based on mutual information of image features. Comput. Electr. Eng. **37**(5), 744–756 (2011)
26. Petrović, V.S., Xydeas, C.S.: Sensor noise effects on signal-level image fusion performance. Inf. Fusion **4**(3), 167–183 (2003)
27. Han, Y., Cai, Y., Cao, Y., Xu, X.: A new image fusion performance metric based on visual information fidelity. Inf. Fusion **14**(2), 127–135 (2013)

28. Li, S., Kang, X., Hu, J.: Image fusion with guided filtering. IEEE Trans. Image Process. **22**, 2864–2875 (2013)
29. Du, J., Li, W., Xiao, B.: Union Laplacian pyramid with multiple features for medical image fusion. Neurocomputing **194**, 326–339 (2016)
30. Liu, Y., Chen, X., Cheng, J., Peng, H.: A medical image fusion method based on convolutional neural networks. In: Proceedings of the 2017 20th International Conference on Information Fusion (Fusion), pp. 10–13 (2017)
31. Zhu, Z., Chai, Y., Yin, H., Li, Y., Liu, Z.: A novel dictionary learning approach for multi-modality medical image fusion. Neurocomputing **214**, 471–482 (2016)